ISSN 2075-1087, Gyroscopy and Navigation, 2018, Vol. 9, No. 4, pp. 287–300. © Pleiades Publishing, Ltd., 2018.
Original Russian Text © I.V. Belokonov, I.A. Timbai, P.N. Nikolaev, 2018, published in Giroskopiya i Navigatsiya, 2018, No. 3, pp. 61–91.

Analysis and Synthesis of Motion of Aerodynamically Stabilized Nanosatellites of the CubeSat Design

I. V. Belokonov[a], *, I. A. Timbai[a], and P. N. Nikolaev[a]

[a]*Inter-University Department of Space Research, Samara National Research University, Samara, Russia*

**e-mail: space@ssau.ru*

Received March 2, 2018

Abstract—The motion of aerodynamically stabilized nanosatellites of the CubeSat design is studied. The features of the nanosatellites behavior in low orbits are conditioned both by the atmospheric effects and their own mass and inertial characteristics: the lifetime of nanosatellites is shorter, while the angular acceleration generated by the aerodynamic moment is much higher as compared with big satellites having large mass. CubeSats may experience resonance modes of motion caused by the shape factor of a rectangular parallelepiped. In addition, the existing commercial CubeSat deployers often generate large initial angular velocities that are random in nature. The conditions that cause the specific features of the CubeSat motion are considered and analyzed. A probabilistic approach to choosing their mass and inertial characteristics is proposed. The problems of motion stabilization are studied, and recommendations are formulated on the design of aerodynamically stabilized CubeSats with a passive/active magnetic damping system.

Keywords: nanosatellite, motion control, aerodynamic stabilization

DOI: 10.1134/S2075108718040028

INTRODUCTION

Creation of nanosatellites is a dominant trend in the development of space technology at the present time. Though a large amount of research on the analysis and synthesis of spacecraft motion has been conducted since the beginning of the space era, the emergence of a new class of space technology—nanosatellites, in particular, CubeSats—requires revision of the fundamentals of their dynamics and motion control. The latter depend on a number of features resulting from the totality of such factors as geometric dimensions, parallelepiped shape factor, mass and inertial characteristics, putting into orbit (low orbits with the dominating influence of aerodynamic forces), the conditions for launching into orbit as secondary payloads on launch vehicles (large angular velocities after CubeSats leave their launch containers).

Analysis of CubeSat motion involves a study and identification of their motion features in low orbits, which generates a need for a probabilistic approach to studying motion relative to the center of mass.

Synthesis of the CubeSat motion is taken to mean a targeted selection of the main mass and inertial characteristics capable of providing the required attitude of nanosatellites under dominant aerodynamic acceleration and strict limitations on CubeSat-borne energy resources. After this problem is successfully solved, the authors propose to use the traditional approach to the formation of a closed control loop aimed at damping the random vector of the initial angular momentum generated after separation.

It should be noted that the CubeSat design features cause the conditions for the emergence of a rather complicated resonant motion. Disregard of these factors and the lack of recommendations to prevent their occurrence can make the target flight mission, associated with specified orientation and stabilization of motion, unfeasible.

All these issues are especially relevant for low-orbit nanosatellites launched into orbits such as those of the International Space Station and lower, the ones that require aerodynamic stabilization, which is the main object of research in this work.

The integrated approach proposed in this paper to solve the above-mentioned problems is original and nothing of this kind has been discussed in literature.

The work includes three interrelated lines of research:

—analysis of the CubeSat motion in low orbits;

—synthesis of design parameters for low-orbit CubeSats;

—synthesis of a closed loop to control angular motion of aerodynamically stabilized nanosatellites.

The authors give examples of practical application of the research results to the design of aerodynamically stabilized nanosatellites. Since 2014, two 3U CubeSats have been developed at Samara University. The first

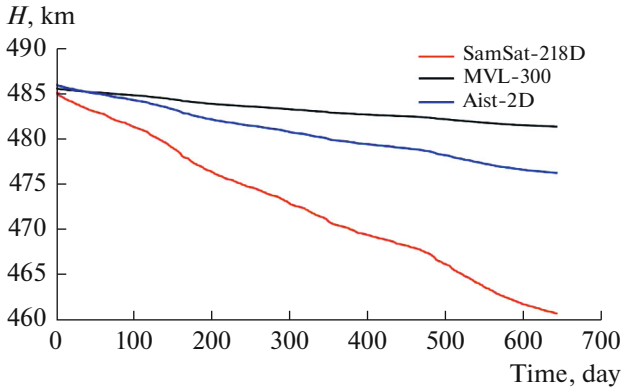

Fig. 1. Orbital altitude variations of the satellites MVL-300, Aist-2D, and the SamSat-218D nanosatellite in the course of 22 months.

nanosatellite SamSat-218D [1] was designed to develop and test the technology of creating a closed control loop for its spatial orientation with a large static stability margin. The second nanosatellite SamSat-QB50 [2] was designed in the framework of an international university project as part of a CubeSat group to study the Earth's troposphere [3]. The technology for synthesizing design parameters used in this project was based on the artificial creation of the required static stability margin due to the transformation of the structure and deployment of an aerodynamic stabilizer.

The presented materials will be useful not only to specialists in the spacecraft dynamics, but they will also help novice designers of university nanosatellites who do not have much practical experience in the field of space technology development.

ANALYSIS OF THE CUBESAT MOTION IN LOW ORBITS

The task of crucial importance in the development of any spatial orientation system is to study uncontrolled motion of a nanosatellite relative to its center of mass because the design conditions of angular motion are provided only at the design stage by selecting its design parameters and setting limits on initial angular velocities generated by the separation system or the end of operation of the preliminary damping system.

Consider the features of the nanosatellite motion in low orbits revealed as a result of the study.

(1) For a nanosatellite, the value of the ballistic coefficient is greater than that of a satellite with larger dimensions and mass (with the same mass density value), which reduces its lifetime in orbit. This makes it possible, taking into consideration a short period of nanosatellite active operation (usually from six to twelve months), to effectively use low orbits, avoiding littering of the near-Earth space.

To illustrate this conclusion, we compare the ballistic coefficients of a 1U CubeSat ($0.1 \times 0.1 \times 0.1$ m^3) and a mini-satellite of cubic shape, the linear dimensions of which are N times larger than those of 1U CubeSat. As is known, assuming that the flow around the satellite is free-molecular and the impact of the gas molecules is absolutely inelastic, it is possible to determine the ballistic coefficient of the satellite by the formula $\sigma_x = c_0 A/m$, where $c_0 = 2.2$ is the drag coefficient, A is the area of the satellite projection onto the plane perpendicular to the velocity vector of the incident flow, m is the satellite mass [4]. Then, the ratio of the 1U CubeSat ballistic coefficients σ_c and those of the mini-satellite under consideration σ_m is determined by the N-fold inverse ratio of their mass density values γ_c and γ_m, respectively. This ratio can be written as $\sigma_c/\sigma_m = N(\gamma_m/\gamma_c)$. It should be noted that the mass density values of small satellites is usually higher than that of large-sized satellites.

Figure 1 shows orbital altitude variations of the satellites MVL-300 and Aist-2D, and the SamSat-218D nanosatellite in the course of 22 months. These spacecraft were launched into a near-circular orbit at a time with an average altitude of $H = 486$ km from the Vostochny Cosmodrome on April 28, 2016. The data is based on the processing of data from TLE files of the NORAD system [5].

As can be seen from the graphs, the decrease in the altitude of the SamSat-218D nanosatellite is 2.5 times larger than that of the Aist-2D satellite and it is 5.8 times larger than that of the MVL-300. At the same time, these numerical ratios are approximately valid for the averaged values of the ballistic coefficients.

(2) The angular acceleration of a nanosatellite caused by the aerodynamic moment is much higher than that of a satellite with large dimensions and mass (with the same values of the relative static stability margin and mass density value). This extends the range of altitudes at which the aerodynamic moment acting on the nanosatellite is significant and it can be used for passive stabilization along the velocity vector of the center of mass motion.

For example, the ratio of the angular accelerations caused by the aerodynamic moment of a 1U CubeSat and those of a minisatellite whose linear dimensions are N times larger than those of the 1U CubeSat is determined by the N^2-fold inverse ratio of their mass density values (with the same values of the relative static stability margin).

For example, Fig. 2 shows the ranges of altitudes H and the relative static stability margins $\Delta\bar{x} = \Delta x/l$ (Δx is the static stability margin, l is the characteristic length of the nanosatellite), where the aerodynamic moment M_a exceeds the gravitational moment M_g for a 3U CubeSat nanosatellite (Fig. 2a) and a minisatellite

(Fig. 2b) whose dimensions are 10 times larger than those the 3U CubeSat (calculations were carried out for the standard atmosphere [6]). Note that for the SamSat-218D satellite at the flight altitude of $H = 486$ km, the ratio of the maximum values of the moments M_a/M_g is equal to 2.3, for the SamSat-QB50 satellite at the flight altitude of $H = 405$ km, the ratio of M_a/M_g is equal to 10.

(3) It should be taken into consideration that the existing commercial deployers—separation systems of nanosatellites—generate large initial angular velocity values (for example, in the QB50 project, the separation systems generate angular velocities of nanosatellites of up to 50°/s after they leave the deployer).

In addition, when nanosatellites are launched from platforms with uncontrolled motion, it is necessary to take into account the random nature of the platform angular motion as well. For example, after the separation of the main payload, the upper stage of the Soyuz carrier rocket performs a regular precession with random values of the orientation angles and angular velocities [7, 8]. Thus, if this stage is used for a piggyback launch of nanosatellites, then, after separation, they usually acquire a significant angular momentum, which subsequently needs to be damped.

(4) It should be also kept in mind that nanosatellites flying in low orbits may experience the emergence of resonant motion. For CubeSats in the form of a rectangular parallelepiped, the aerodynamic moment depends on the spatial angle of attack and the angle of proper rotation [9], which, as will be shown below, creates the prerequisites for the resonance, which manifests itself in a sharp change in the amplitude of oscillations along the angle of attack, when the integer combination of the oscillation frequency of the spatial angle of attack and the mean frequency of proper rotation is close to zero.

The above features of the nanosatellite motion in low orbits generate a need for a probabilistic approach to studying motion with regard to the center of mass. Below are the results of the studies obtained by the authors within the framework of this approach.

It is assumed that the nanosatellite is a dynamically symmetrical rigid body, the flow is of free-molecular nature, the impact of gas molecules is absolutely inelastic so that the resultant of the aerodynamic forces is applied to the nanosatellite geometric center. In this case, the aerodynamic drag force is determined by the area of the nanosatellite projection onto the plane perpendicular to the velocity vector of the incident flow, and the aerodynamic angular acceleration (torque characteristic) of the CubeSat is determined by the formula [9]:

$$M_\alpha(\alpha, \varphi, H) = m_0(H) \times \left(|\cos\alpha| + k_s \sin\alpha\left(|\sin\varphi| + |\cos\varphi|\right)\right)\sin\alpha, \quad (1)$$

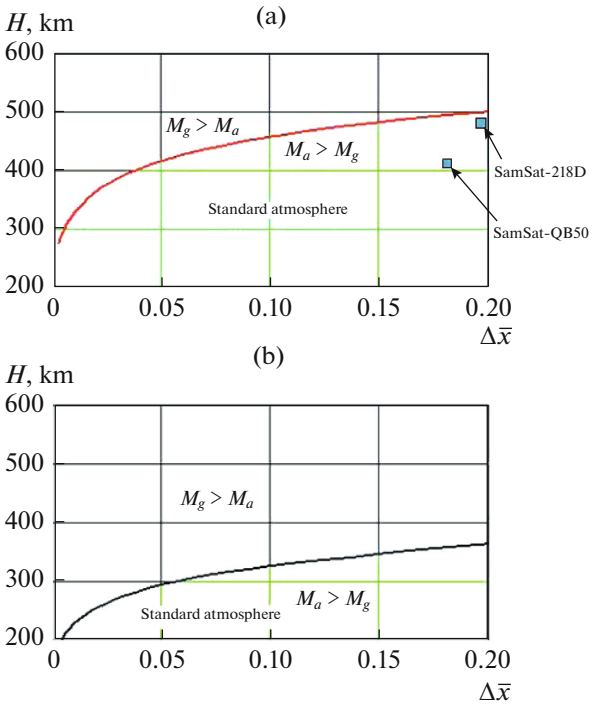

Fig. 2. The range of altitudes H and the relative static stability margin $\Delta\bar{x}$, where the aerodynamic moment M_a exceeds the gravitational moment M_g for (a) a 3U CubeSat nanosatellite and (b) a satellite whose dimensions are 10 times larger than those of the 3U CubeSat nanosatellite.

where $m_0(H) = -\Delta\bar{x}c_0 Slq(H)/J_n$, α is the spatial angle of attack, φ is the angle of proper rotation, k_s is the ratio of the area of one of the lateral surfaces to the reference area, S is the reference area of the nanosatellite, $q(H) = \rho(H)[V(H)]^2/2$ is the velocity pressure, H is the flight altitude, $\rho(H)$ is the atmosphere density, $V(H) = \sqrt{k_E/(R_E + H)}$ is the flight speed, k_E is the Earth's gravity parameter, R_E is the Earth's radius, J_n is the nanosatellite transverse moment of inertia ($J_y = J_z = J_n$).

To analyze the angular motion of nanosatellites in the nonresonant case of motion, the moment characteristic (1) can be averaged over the angle of proper rotation:

$$M_\alpha(\alpha, H) = m_0(H)\left(|\cos\alpha| + k_s\frac{4}{\pi}\sin\alpha\right)\sin\alpha, \quad (2)$$

and approximated, for the approximate analysis of the angular motion, by the sinusoidal dependence on the angle of attack:

$$M_\alpha(\alpha, H) = a(H)\sin\alpha, \quad (3)$$

where $a(H) = m_0(H)a_{nk}$; $a_{nk} = 1.51$ at $k_s = 1$; $a_{nk} = 2.59$ at $k_s = 2$; $a_{nk} = 3.67$ at $k_s = 3$.

To analyze the angular motion of nanosatellites in the resonant case of motion, assuming that in Formula (1) $|\sin\varphi| + |\cos\varphi| \approx 1 + |\sin 2\varphi|/(1+\sqrt{2})$ (maximum error 0.015), we can represent the moment characteristic (1) as two terms: the first and the main one, depending on the spatial angle of attack and flight altitude, and the second term, depending on the spatial angle of attack, the angle of proper rotation and flight altitude, assigning small parameter ε to it:

$$M_\alpha(\alpha, \varphi, H) = M_\alpha(\alpha, H) + \varepsilon\Phi_\alpha(\alpha, \varphi, H), \quad (4)$$

where

$$M_\alpha(\alpha, H) = m_0(H)\left(|\cos\alpha| + k_s \sin\alpha\right)\sin\alpha, \quad (5)$$

$$\Phi_\alpha(\alpha, \varphi, H) = m_0(H)k_s \frac{|\sin 2\varphi|}{1+\sqrt{2}}\sin^2\alpha. \quad (6)$$

For an approximate analysis of the angular motion of nanosatellites in the resonant case of motion, the relation (5) can also be approximated by a sinusoidal dependence on the angle of attack:

$$M_\alpha(\alpha, H) = m_0(H)m_{nk}\sin\alpha, \quad (7)$$

where $m_{nk} = 1.27$ at $k_s = 1$; $m_{nk} = 2.12$ at $k_s = 2$; $m_{nk} = 2.97$ at $k_s = 3$.

To obtain the analytical laws of the angle-of-attack distribution, we used an approximate model of angular motion in the plane of a circular orbit relative to the trajectory coordinate system. The model describes the change in the angle of attack (under the action of the gravitational and aerodynamic restoring moments) by the equation of the form [4]:

$$\ddot{\alpha} - a(H)\sin\alpha - c(H)\sin 2\alpha = 0, \quad (8)$$

where $a(H) = m_0(H)\,a_{nk}$ is the coefficient in the moment characteristic (3) due to the aerodynamic restoring moment; $c(H) = 3(J_n - J_x)(\omega_{\text{orb}}(H))^2/(2J_n)$ is the coefficient due to the gravitational moment; J_x is the nanosatellite longitudinal moment of inertia; $\omega_{\text{orb}}(H) = \sqrt{k_E/(R_E + H)^3}$ is the nanosatellite center-of-mass angular velocity in orbit.

The change in the altitude of the circular orbit due to the atmosphere resistance is very slow, therefore, when considering the angular motion of a nanosatellite for one or several turns, the flight altitude can be assumed constant ($H = \text{const}$). In this case, for the system (8), the energy integral is valid:

$$\dot{\alpha}^2/2 + a\cos\alpha + c\cos^2\alpha = E_0, \quad (9)$$

where $E_0 = a\cos\alpha_0 + c\cos^2\alpha_0 + \dot{\alpha}_0^2/2$ is defined in terms of the initial conditions of motion.

The magnitude of the maximum angle of attack of a nanosatellite under oscillations can be found from the energy integral (3) with $\dot{\alpha} = 0$, assuming that $H = \text{const}$:

$$\cos\alpha_{\max} = -\frac{a}{2c} - \sqrt{\left(\frac{-a}{2c}\right)^2 + \frac{a}{c}\cos\alpha_0 + \cos^2\alpha_0 + \frac{\dot{\alpha}_0^2}{2c}}. \quad (10)$$

When the nanosatellite is separated from the deployer, the realization of the maximum angle-of-attack value is of a random nature. The latter is determined by the values of the aerodynamic and gravitational moments and the initial values of the angle of attack α_0 and angular velocity $\dot{\alpha}_0$.

Proceeding from the above features of nanosatellite launching into orbit, it is assumed that the initial angular velocity $\dot{\alpha}_0$ has the greatest spread in the values among the terms included in (10). Then, under the condition that the spreads in the other terms are neglected, we find the distribution laws of the maximum angle-of- attack values for the two most common variants of the $\dot{\alpha}_0$ modulus distribution laws. If the modulus of $\dot{\alpha}_0$ is distributed according to the Rayleigh law (the scale distribution parameter $\sigma > 0$), then the distribution function of the maximum angle of attack is determined by the formula [9]:

$$F(\alpha_{\max}) = 1 - \exp\left(\frac{-a(\cos\alpha_{\max} - \cos\alpha_0) - c(\cos^2\alpha_{\max} - \cos^2\alpha_0)}{\sigma^2}\right). \quad (11)$$

If the modulus of $\dot{\alpha}_0$ is distributed uniformly in the range of $[0, \dot{\alpha}_{0\max}]$, then the distribution function of the maximum angle of attack is determined by the formula [9]:

$$F(\alpha_{\max}) = \frac{\sqrt{2a(\cos\alpha_{\max} - \cos\alpha_0) + 2c(\cos^2\alpha_{\max} - \cos^2\alpha_0)}}{\dot{\alpha}_{0\max}}. \quad (12)$$

The error in using the analytical distribution functions of the maximum angle of attack (11) and (12) with $c = 0$ for the case of spatial motion has been estimated. As an example, we considered the motion of a

3U CubeSat with dimensions $0.1 \times 0.1 \times 0.3$ m^3, the longitudinal moment of inertia $J_x = 0.0033$ kg m^2, the transverse moment of inertia $J_n = 0.012$ kg m^2, the distance between the pressure center, and the center of mass with $\Delta x = 0.055$ m (which corresponds approximately to the characteristics of the SamSat-QB50 nanosatellite after the deployment of the aerodynamic stabilizer). The graphs in Fig. 3 are given for the case when the components of the initial transverse angular velocity are distributed in accordance with the normal law $3\sigma_{\omega_y} = 3\sigma_{\omega_z} = 2.5$ deg (which approximately corresponds to the characteristics of the launch container manufactured by Space Rocket Center Progress [10]), for the flight altitude $H = 330$ km and the initial angle of attack $\alpha_0 = 15$ deg. We can see the graph of the analytical distribution function (11) (curve *1*) and the graphs of the distribution function of the maximum angle of attack α_{max} obtained in the numerical experiments using a complete system of differential equations describing the spatial motion of the nanosatellite with respect to the center of mass [4] (curve *2* for $3\sigma_{\omega_x} = 0.5$ deg/s, curve *3* for $3\sigma_{\omega_x} = 1.5$ deg/s, curve *4* for $3\sigma_{\omega_x} = 2.5$ deg/s).

As follows from the results obtained, when the nanosatellite separates along the center-of-mass velocity vector (at small initial values of the angle of attack) and with a slight twist relative to the longitudinal axis, in the case of spatial motion, we can use, with sufficient accuracy, analytical distribution functions of the maximum angle of attack obtained for the case of plane angular motion.

Earlier we pointed out the possibility of emergence of resonant modes of motion of CubeSat nanosatellites when, with a decrease in the orbit altitude due to atmospheric drag, the integer combination of the oscillation frequency of the spatial angle of attack and the mean frequency of proper rotation may be close to zero. Resonant modes of spacecraft motion in the atmosphere were studied in [11–13], which consider space vehicles intended for uncontrolled descent in the atmosphere, the ones that are usually referred to as a class of axisymmetric bodies. In this paper, we analyze the possibility of emergence of the resonant motion mode of CubeSat nanosatellites during orbital flights, caused by the shape factor of a rectangular parallelepiped.

In the case when the aerodynamic moment is predominant and determines the character of the angular motion, it tends to align the longitudinal axis of the nanosatellite with the direction of the incident flow. However, this is counteracted by the gyroscopic forces that cause forced precession of the angular momentum vector with respect to the velocity vector of the center of mass. The precession of the satellite's longitudinal axis with respect to the center-of-mass velocity vector (within the time interval equal to the period of a turn), opposite in direction to the velocity vector, is called "inverse" precession, while the one coinciding with the direction of the velocity vector is called "direct" precession [14]. When the condition of $R > G$ is satisfied, "inverse" precession is realized, while "direct" precession is realized with $G > R$, where and $G = R\cos\alpha + (\omega_y \sin\varphi + \omega_z \cos\varphi)\sin\alpha$, $R = \bar{J}_x\omega_x$ are the projections of the angular momentum vector on the longitudinal axis of the nanosatellite and on the direction of the center-of-mass velocity, divided by the transverse moment of inertia J_n; $\bar{J}_x = J_x/J_n$; $\omega_x, \omega_y, \omega_z$ are the projections of the angular velocity vector of the nanosatellite on the axes of the body-fixed coordinate system.

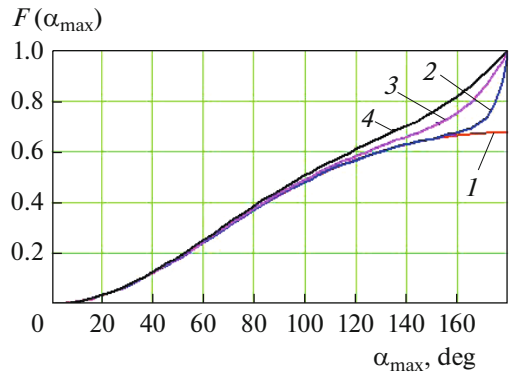

Fig. 3. Maximum angle-of-attack distribution function.

In the case of unperturbed motion ($\varepsilon = 0$, $H = \text{const}$, $R = \text{const}$, $G = \text{const}$), the solution for the spatial angle of attack in the case of a sinusoidal moment characteristic (7) was obtained in [15] in the following form:

$$\cos\alpha = A_1 cn^2\left[\frac{yK}{\pi} + K, k\right] + x, \qquad (13)$$

where $cn(u)$ is the elliptic cosine, $x = \cos\alpha_{max}$, $y = \omega(t - t_0)$, $\omega = \pi\beta/K$ is the oscillation frequency, $A_1 = x_2 - x$, $K(k)$ is a complete elliptic integral of the first kind, $k = \sqrt{A_1/(2\eta)}$ is the modulus of elliptic functions, $\beta = \sqrt{-m_0 m_{nk}\eta}$, $x_2 = \cos\alpha_{min} = \eta - (a - bx)/(1 - x^2)$, $a = (R^2 + G^2)/(-4m_0 m_{nk})$, $b = RG/(-2m_0 m_{nk})$, $\eta = \sqrt{1 - 2(ax - b)/(1 - x^2) + [(a - bx)/(1 - x^2)]^2}$.

For small values of the modulus of elliptic functions k, formula (13) is simplified [12]:

$$\cos\alpha \approx a_1 + b_1\cos y, \qquad (14)$$

where $a_1 = (x + x_2)/2$, $b_1 = -(x_2 - x)/2$.

The average frequency of proper rotation is defined as

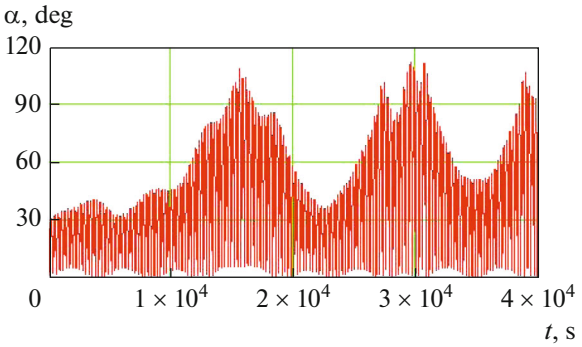

Fig. 4. Dependence of the 3U CubeSat spatial angle of attack on time.

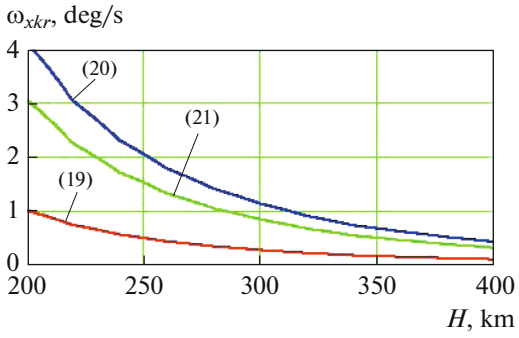

Fig. 5. The relations between the critical value of the nanosatellite longitudinal angular velocity and the flight altitude at which the conditions for the emergence of the nanosatellite resonant motion are fulfilled.

$$\lambda \approx R(1/\bar{J}_x - 1/2) + \mathrm{sgn}(R-G)\sqrt{\omega_a^2 + \frac{R^2}{4}}, \qquad (15)$$

where $\omega_a = \sqrt{-m_0 m_{nk}}$.

The frequency of oscillations along the spatial angle of attack is given by

$$\omega \approx 2\sqrt{\omega_a^2 + \frac{R^2}{4}}. \qquad (16)$$

In perturbed motion, resonances manifest themselves when the condition [16] is satisfied:

$$m\omega - n\lambda = O(\varepsilon), \qquad (17)$$

where m, n are coprime integers.

Ratios of resonance frequencies can be obtained by calculating the mean power introduced into the system by the exciting moment over time T during which it has no time to change the shape of the oscillations [16]:

$$\frac{1}{T}\int_{t_0}^{t_0+T} \Phi_\alpha(\alpha, \varphi, H)\dot{\alpha}dt. \qquad (18)$$

Taking into account (6) and (14), analyzing the solution (18), we obtain the conditions for the emergence of resonances in the following cases: if the initial motion corresponds to a "direct" precession $G > R$, then the system has resonance frequency ratios, corresponding to the conditions $\omega = -4\lambda$, $\omega = 2\lambda$, $\omega = 4\lambda$; if the initial motion corresponds to an "inverse" precession $R > G$, then the system has a resonant frequency ratio $3\omega = 4\lambda$.

Taking into account the expressions for the frequencies (15), (16), we obtain the formulas for determining the critical value of the longitudinal angular velocity of the nanosatellite under which the conditions for the emergence of resonant motion are satisfied:

—for the frequency ratio of $\omega = -4\lambda$ and $3\omega = 4\lambda$:

$$\omega_{xkr} = \frac{1}{2}\sqrt{\frac{\omega_a^2}{1 - \bar{J}_x + \frac{3}{16}\bar{J}_x^2}}; \qquad (19)$$

—for the frequency ratio of $\omega = 2\lambda$:

$$\omega_{xkr} = 2\sqrt{\frac{\omega_a^2}{1 - \bar{J}_x - \frac{3}{4}\bar{J}_x^2}}; \qquad (20)$$

—for the frequency ratio of $\omega = 4\lambda$:

$$\omega_{xkr} = \frac{3}{2}\sqrt{\frac{\omega_a^2}{1 - \bar{J}_x - \frac{5}{16}\bar{J}_x^2}}. \qquad (21)$$

As an example, Fig. 4 shows the resonant variation in the spatial angle of attack of a 3U CubeSat with the typical values of moments of inertia $J_x = 0.005$ kg m^2, $J_n = 0.025$ kg m^2 and the static stability margin $\Delta x = 0.05$ m, corresponding to that of SamSat-218D, with the following initial motion conditions: the initial flight altitude $H = 270$ km, the initial value of the spatial angle of attack $\alpha_0 = 30$ deg, longitudinal angular velocity $\omega_x = 0.4$ deg/s.

Figure 5 shows the relations between the critical value of the longitudinal angular velocity and the flight altitude for the same nanosatellite at which the conditions for the emergence of the resonant motion (19)–(21) are fulfilled.

Resonant modes of nanosatellite motion can be avoided by setting a limit on the value of the longitudinal angular velocity during the nanosatellite separation from the deployer, and also by early initiation of the stabilization system in order to break the resonant frequency ratio.

SYNTHESIS OF DESIGN PARAMETERS FOR LOW-ORBIT CUBESAT

In the publications known to the authors, the problem of ensuring aerodynamic stabilization of nanosatellites is solved in a deterministic formulation. For example, in [17] this problem was solved for a CubeSat by deploying solar panels at a certain angle to its longitudinal axis after it was separated from the launcher. In this paper, based on the results of the analysis of the nanosatellite motion in low orbits, the authors consider this problem in a probabilistic formulation with respect to the angular motion of the nanosatellite after it was separated from the launcher.

The analytical laws of distribution of the maximum angle of attack (11) and (12) were used to derive the formulas for selecting design parameters (static stability margin, geometric dimensions, transverse moment of inertia) of an aerodynamically stabilized nanosatellite in order to ensure, in low Earth orbits, a deviation of the nanosatellite longitudinal axis from the center-of-mass velocity vector, which should be less than a permissible value, with a given probability at a required altitude for given spreads in the angular velocity caused by the separation system. However, if a combined stabilization system is used, it is necessary to take into account the spreads in the angular velocities by the time the active system of preliminary damping finishes working. For example, if we need the maximum angle of attack of a CubeSat to be less than the permissible value $\alpha^*_{\max}$ with a probability of no less than p^* at the altitudes where the aerodynamic moment significantly exceeds the gravitational one, the following condition for the design parameter d of the nanosatellite must be fulfilled [18]:

—in the case when the value of the initial angular velocity $\dot\alpha_0$ corresponds to the Rayleigh distribution,

$$d = \frac{\Delta x}{J_n} lb \geq \frac{\pi\sigma^2 \ln(1-p^*)}{4c_0(\cos\alpha^*_{\max} - \cos\alpha_0)q(H)}; \qquad (22)$$

—in the case when the initial angular velocity $\dot\alpha_0$ is distributed in accordance with the uniform law within the range $[0, \dot\alpha_{0\max}]$:

$$d = \frac{\Delta x}{J_n} lb \geq \frac{\pi(\dot\alpha_{0\max}p^*)^2}{8c_0(\cos\alpha_0 - \cos\alpha^*_{\max})q(H)}, \qquad (23)$$

where b is the side of the rectangular parallelepiped base.

Using (22), (23), we formed a set of nomograms that allowed the synthesis of design parameters of aerodynamically stabilized CubeSat nanosatellites. The right-hand parts in Figs. 6 and 7 give the dependencies of the required design parameter d of the nanosatellite on the orbit altitude H and the value of parameter σ (the value of the initial transverse angular velocity has the Rayleigh distribution) for the values of the maximum angle of attack $\alpha^*_{\max} = 20$ deg (Fig. 6) and $\alpha^*_{\max} = 30$ deg (Fig. 7) of the probability $p^* = 0.95$ and the initial angle of attack $\alpha_0 = 0$. The left-hand parts in Figs. 6 and 7 give the dependences of the 3U CubeSat design parameter values for different values of the transverse moment of inertia on the static stability margin Δx. Also indicated there is the design parameter value of the aerodynamically stabilized SamSat-QB50 nanosatellite of the transformable construction, weighing 2 kg, having the initial shape of a 2U CubeSat with the dimensions of $0.1 \times 0.1 \times 0.2$ m^3 and the initial distance between the pressure center and the center of mass $\Delta x = 0.02$ m. After separation from the launcher, the nanosatellite is transformed into a 3U CubeSat with dimensions of $0.1 \times 0.1 \times 0.3$ m^3, which significantly increases the distance between the pressure center and the center of mass to $\Delta x = 0.055$ m, and, consequently, aerodynamic moment. Calculations were carried out for the standard density of the atmosphere in accordance with [6].

Nomograms can be used both to select the design parameters of the nanosatellite, focusing on the existing aids of separation, and to specify the requirements for permissible errors in the separation system of the already manufactured nanosatellite. Figure 6 shows a sequence of choosing the nanosatellite parameters for the orbit height $H = 380$ km with given constraints on the conditions of motion relative to the center of mass formed by the target flight task: $\alpha^*_{\max} = 20$ deg, $p^* = 0.95$, $\alpha_0 = 0$, $\sigma = 0.05$ deg/s. As can be seen, the value of the nanosatellite design parameter needed to ensure the specified motion must meet the condition of $d \geq 0.13$ m/kg (right side of the figure), the design parameters are selected on the basis of the left part of the figure. Figure 7 shows an example of setting the requirements for the error in the operation of the onboard angular velocity damping system for the SamSat-QB50 orbiting at $H = 380$ km and the conditions $\alpha^*_{\max} = 30$ deg, $p^* = 0.95$, $\alpha_0 = 0$ for the target flight mission.

As can be seen, in order for the SamSat-QB50 to perform a specified motion, it is necessary that the requirement for the value of the transverse angular velocity $\sigma \leq 0.08$ deg/s be satisfied, which must be fulfilled after the damping process is completed and the satellite is brought into operation.

The proposed approach to choosing design parameters of the aerodynamically stabilized CubeSat nanosatellite was granted the Eurasian patent [19].

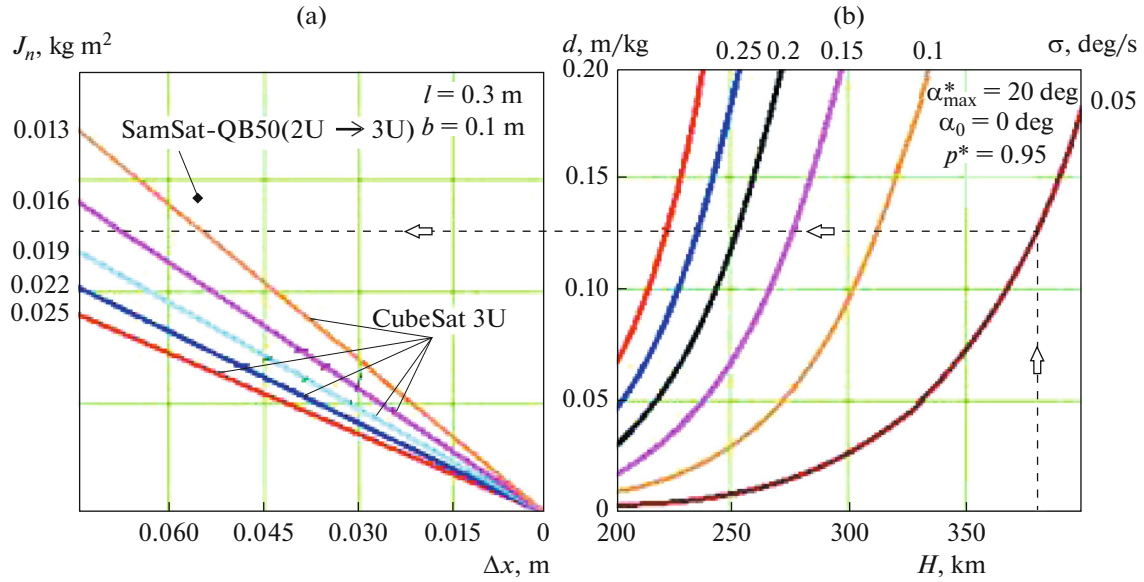

Fig. 6. Nomogram for selecting the design parameter of the 3U CubeSat, depending on the flight altitude H and the value of parameter σ at $\alpha^*_{max} = 20°$, $p^* = 0.95$, $\alpha_0 = 0$.

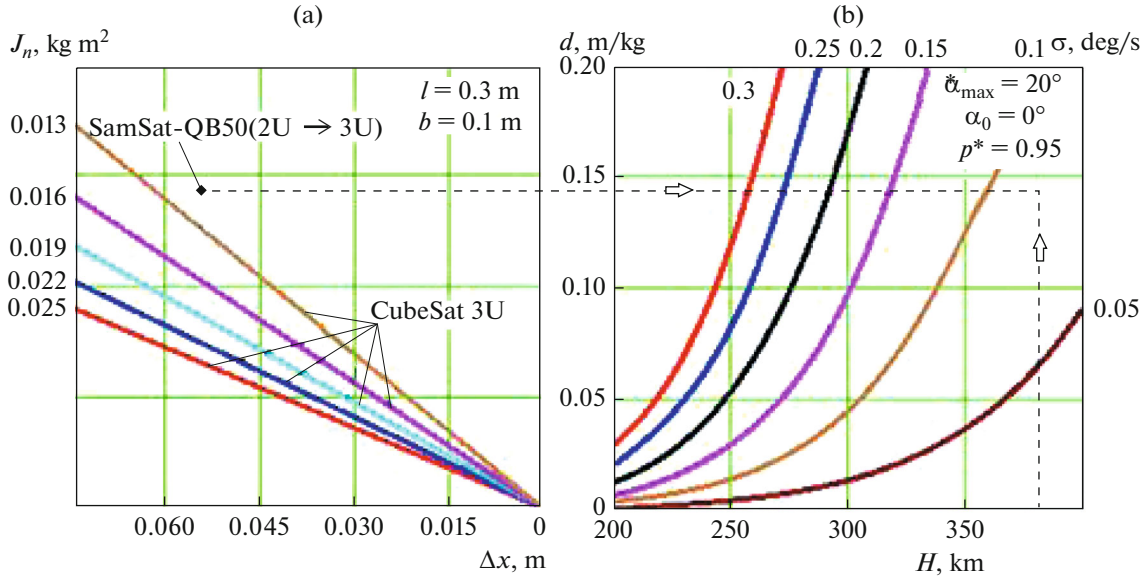

Fig. 7. Nomogram for selecting the design parameter of the 3U CubeSat, depending on the flight altitude H and the value of parameter σ at $\alpha^*_{max} = 30°$, $p^* = 0.95$, $\alpha_0 = 0$.

SYNTHESIS OF A CLOSED LOOP TO CONTROL THE ANGULAR MOTION OF AERODYNAMICALLY STABILIZED NANOSATELLITES

The problem of the angular motion control of aerodynamically stabilized nanosatellites is largely due to the above-mentioned motion features of nanosatellites of this type, including the initial angular momentum acquired after the nanosatellite separates from the deployer.

The attitude control system of aerodynamically stabilized nanosatellites should provide:

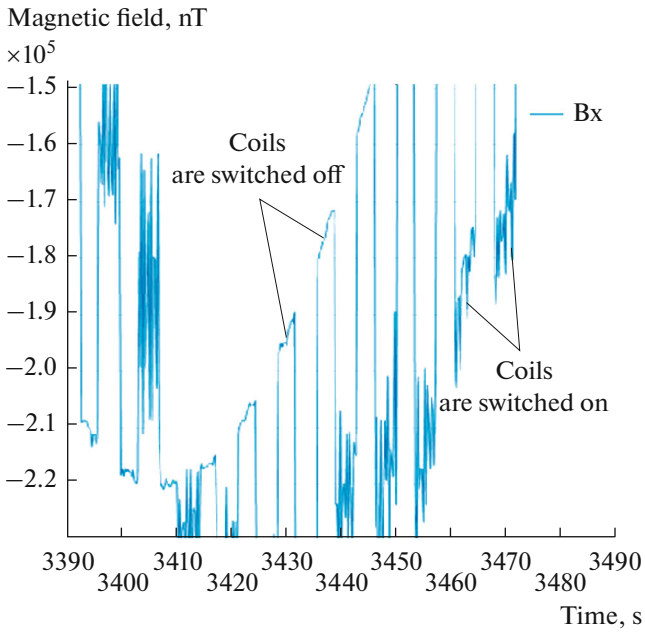

Fig. 8. Changes in the magnetometer data Bx (projection of magnetic field induction vector on axis *X*) caused by switching on and off of the magnetic coils.

.

—damping of initial angular velocities;

—bringing the nanosatellite to a specified attitude related to the vector of the incident flow, which is a stable equilibrium position;

—keeping the nanosatellite in an equilibrium position to ensure the required angular motion conditions.

Since active reorientation of nanosatellites in space is not usually included in their target mission, the above-listed tasks can be solved with the use of magnetic coils as an actuator.

These problems are considered in a large number of publications, among which the monograph [20] occupies a special place. It is a summary review of the studies conducted by a group of scientists, headed by Professor M.Yu. Ovchinnikov, over many years.

Of particular interest for practical use in CubeSats are flat magnetic coils that can be embedded in the substrate of solar panels; they do not occupy the satellite interior and have a small mass [21].

To solve the problem of damping the initial angular velocities (in order to reduce the angular momentum modulus) by means of the active magnetic control system, the B-dot control algorithm [22–24] is usually used, which is simple and reliable, and requires only measurements of the Earth's magnetic field induction vector components. In this case, measurement of the Earth's magnetic field with a magnetometer and generation of control magnetic moments require correct matching of these interdependent and mutually exclusive processes, since the control dipole moment of the

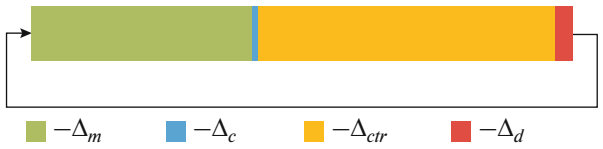

Fig. 9. A cyclogram of the B-dot algorithm operation onboard a nanosatellite.

coil introduces noticeable distortions in the magnetometer measurements due to the satellite small dimensions. Figure 8 shows the results of a full-scale experiment at a test facility, simulating the Earth's magnetic field, with alternate switching of the magnetic coils on and off . The areas of high-frequency variations in the magnetic field induction correspond to the magnetometer readings during the operation of the magnetic control coils, which indicates that they cannot be used in the control algorithm.

The B-dot algorithm forms the required value and direction of the current applied to the magnetic coils in order to generate the dipole moment with a required sign and modulus. In so doing, the generated dipole moment is assumed to be proportional to the Earth's magnetic field induction vector derivative:

$$\bar{m} = -k\dot{\bar{B}}, \tag{24}$$

where $\dot{\bar{B}}$ is the derivative of the Earth's magnetic field induction vector; k is the proportionality coefficient. Then the required value of the current to be fed to the coils is determined from the relation:

$$\bar{J} = -\frac{k}{S}\dot{\bar{B}}, \tag{25}$$

where S is the effective area of the conductor circuit in the coil.

It is appropriate to consider the operation of the active stabilization system based on the B-dot algorithm, which includes the following stages (Fig. 9):

—measurements of the Earth's magnetic field of Δ_m duration;

—calculation of the control magnetic moment of Δ_c duration;

—formation of the control magnetic moment by means of magnetic coils of Δ_{ctr} duration;

—time delay to complete the transient process in the magnetic coils and the disappearance of the control moment of Δ_d duration.

These four time intervals are the parameters of the active stabilization system based on the B-dot algorithm and they require a reasonable choice.

The duration Δ_m of the magnetometer measurement of the Earth's magnetic field induction vector components is chosen from the condition that their derivatives are calculated at the last point of the measurement interval with an accuracy sufficient to form a

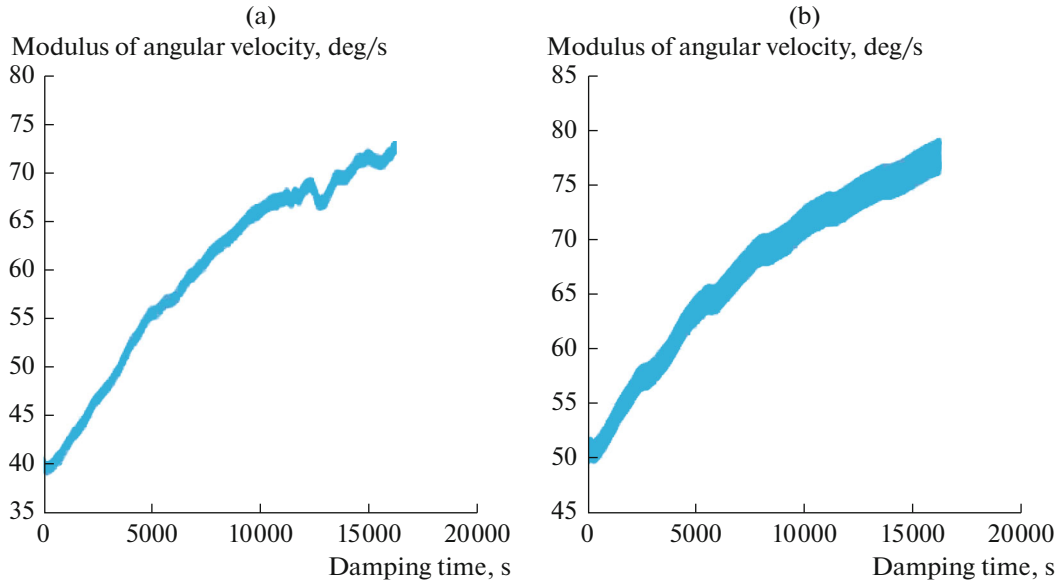

Fig. 10. Change in the angular velocity of a nanosatellite caused by the incorrect choice of the cyclogram parameters at initial angular velocities of 40 deg/s (a) and 50 deg/s (b).

dipole moment which provides damping of the angular motion and depends on the method for calculation of the derivative. Since in the control interval Δ_{ctr} the dipole moment of the coils calculated at the measurement stage of Δ_m is constant in magnitude and direction, the duration of the control interval Δ_{ctr} is chosen in such a way that the vectors $\bar{m}$ and $\dot{\bar{B}}$ are oppositely directed throughout the whole interval, which should exclude the nanosatellite spinning (the algorithm must remove energy from the oscillatory system rather than pump energy). If the duration of the control intervals Δ_{ctr} is chosen incorrectly, the algorithm will result in spinning of the satellite. Figure 10 shows the examples in which the intervals of the magnetometer operation $\Delta_m = 3s$ and the control coil operation $\Delta_{ctr} = 5s$ were chosen incorrectly for the initial modulus of the satellite angular velocity of 40 and 50 deg/s, correspondingly. As a result, the satellite spins up in three turns of orbital motion to angular velocities of 72 and 78 deg/s, respectively.

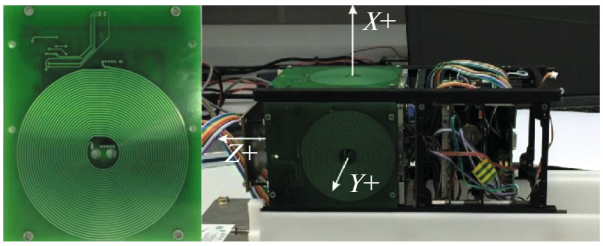

Fig. 11. Magnetic coil (left); the magnetic coils installed on the SamSat-QB50 satellite (right).

The procedure for selecting the parameters of the active magnetic stabilization system is illustrated by an example of the SamSat-QB50 nanosatellite, which is controlled by a system of three orthogonally placed flat magnetic coils (Figure 11). The coils are fabricated as 10-layer boards used as substrates for photoelectronic converters of solar panels (the effective area of the conductor in the coil is 0.5 m^2). As measurement devices, the developed closed control loop contains two three-axis MEMS magnetometers with the measurement range of the magnetic field induction of $\pm$ 4800 μT with a resolution of 150 nT and a mean square deviation $\sigma_B = 1500$ nT.

To implement the B-dot algorithm into practice, the designers have to solve a number of new problems in addition to those mentioned earlier:

—MEMS magnetometers have a large noise component, which makes it difficult to find the derivative of the Earth's magnetic field induction vector at a current time so that the measured values need preliminary smoothing;

—proper account should be taken of the sensor signal decay with a stepwise change in the Earth's magnetic field induction vector caused by the disconnection of the coils at the end of the control interval.

The main difficulty of the B-dot algorithm implementation, which follows from the first item, is to find the derivative Earth's magnetic field induction vector at a current time. This problem was solved in the development of the control algorithm for SamSat-QB50 by smoothing the magnetometer data in all three axes using the least squares method with the help of a second-degree polynomial in the chosen measurement interval:

Table 1. Recommended parameters of the B-dot algorithm: duration of the measurement and control intervals

Angular velocity of the nanosatellite ω, deg/s	Magnetometer time of operation Δ_m, s	Control coil time of operation Δ_{ctr}, s	Damping time, s
90	1.5	1	23000–47000
80	1.5	1	24000–33000
70	1.5	1	15000–25000
60	2	1.5	13000–18000
50	2	2	10000–5000
40	2	3	10000–13500
30	3	4	5000–10000
20	3	4	4000–5000
10	3	4	2000–3000

$$\bar{B}(\tau) = \bar{a}_0 + \bar{a}_1\tau + \bar{a}_2\tau^2,$$

where $(\bar{a}_0, \bar{a}_1, \bar{a}_2)$ are the polynomial coefficients; τ is the moment of time within the measurement interval. The vector of the magnetic field induction derivatives is calculated from the formula:

$$\dot{\bar{B}}(\tau) = \bar{a}_1 + 2\bar{a}_2\tau.$$

Then the control currents are calculated for the end of the measurement interval τ_n from the equation:

$$\bar{J} = -\frac{k}{S}(\bar{a}_1 + 2\bar{a}_2\tau_n).$$

The experimental studies have shown that the are switched off time delay in switching off the coils and switching on and switching on of the magnetometer should be no less than 0.25 s ($\Delta_d \geq 0.25s$) for the coil model used.

Based on the parametric studies of the simulation model of the B-dot algorithm, its parameters (measurement intervals of the magnetometer and control intervals) satisfying the required conditions were chosen (Table 1).

Table 1 presents the parameters of the B-dot algorithm that were used in the SamSat-QB50 control system, the measurement and control intervals were taken to fit the modulus of the initial angular velocity 90 deg/s (the worst case of deployment), based on the recommendations of the QB50 project managers [5]. Figure 12 shows the damping time for the initial angular velocities of 10 and 90 deg/s.

In addition to the active magnetic stabilization system, SamSat-QB50 has a passive magnetic stabiliza-

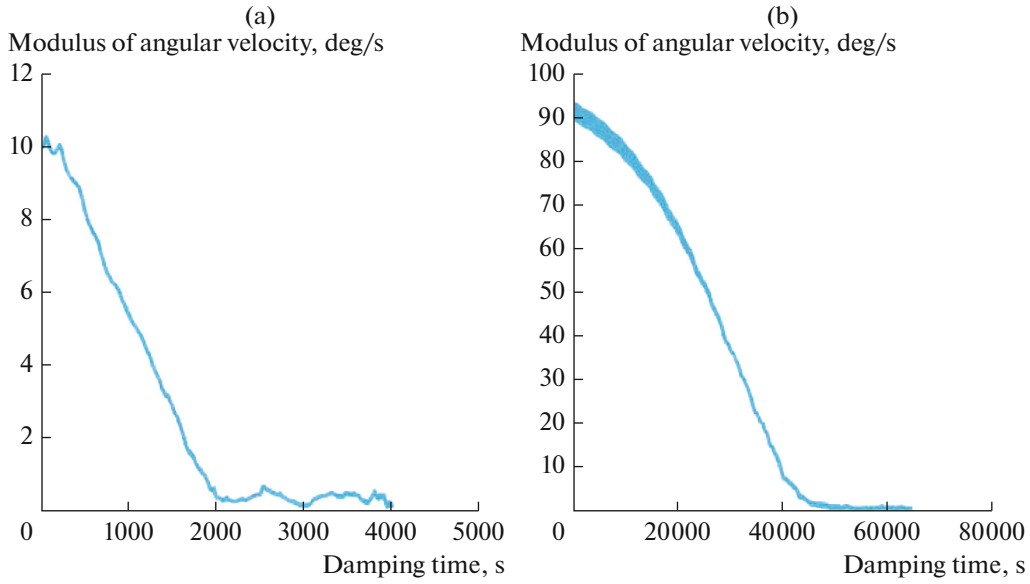

Fig. 12. Damping time of the initial angular velocities for SamSat-QB50: 10 deg/s (a) and 90 deg/s (b).

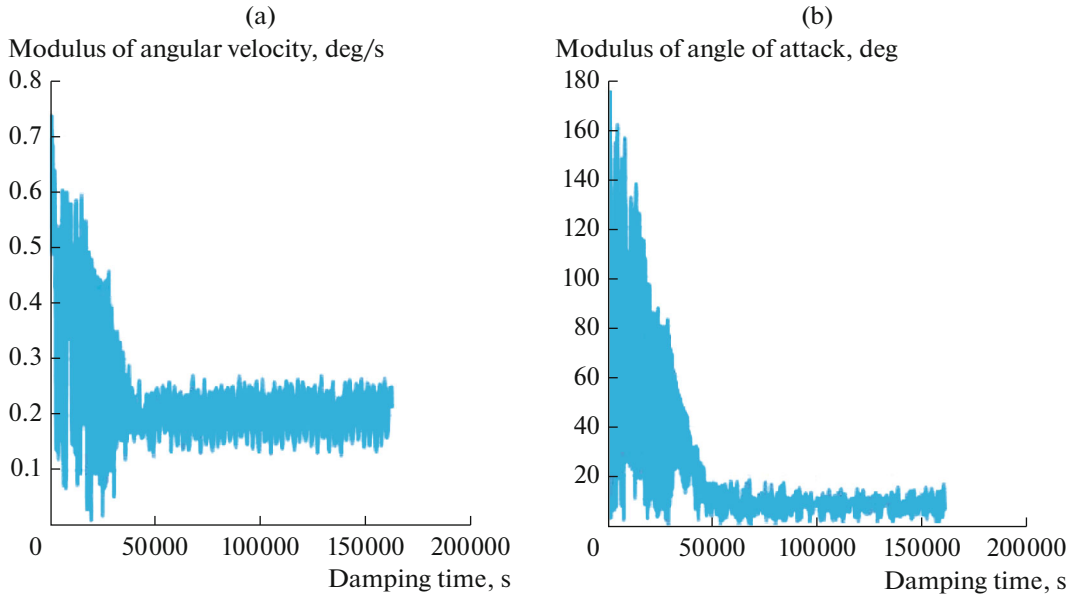

Fig. 13. Changes in the initial angular velocity of 0.5 deg/s due to the hysteresis rods (a); changes in the spatial angle of attack due to the hysteresis rods (b).

tion system with hysteresis rods. This system is intended for precise damping of angular velocities and keeping the nanosatellite in an equilibrium position. The passive magnetic stabilization system on hysteresis rods was developed jointly with the Keldysh Institute of Applied Mathematics, the research team headed by Doctor of Sciences (Physics and Mathematics), Professor M.Yu. Ovchinnikov [25–27]. In this case, under the interaction with the Earth's magnetic field, a dipole magnetic moment is formed on each rod. It is directed along the longitudinal axis of the rod and can be described by the following model:

$$\bar{m} = \frac{\mu V B_r}{\mu_0 H_c}\left(\frac{B_\tau}{\mu_0} - H_c \operatorname{sgn}\dot{B}_\tau\right)\bar{n},$$

where μ is the relative magnetic permeability of the rod; V is the rod volume; B_r is the residual magnetization of the rod; $\mu_0 = 1.2566\times10^{-6}\ H/A^2$ is the magnetic constant; H_c is the coercive force; $B_\tau = \bar{B}\cdot\bar{n}$ is the projection of the Earth's magnetic field induction vector on the longitudinal axis of the rod; $\bar{n}$ is the unit vector along the longitudinal axis of the rod; $\dot{B}_\tau$ is derivative of the projection of the Earth's magnetic field induction vector.

Figure 13 shows the graphs of the angular velocity modulus versus time and the spatial angle of attack versus time after the magnetic coils were disconnected and damped only with the hysteresis rods. It can be noted that the system reaches a steady state, characterized by the deviation of the longitudinal axis from the incident flow vector by the balancing angle, which is approximately 8 degrees, and the residual velocity of 0.2 deg/s, which meet the requirements of the QB50 project.

Better results can be obtained if the parameters of the active damping algorithm are chosen to take into account the influence of the hysteresis rods. Otherwise, the damping interval will be longer. Figure 14 presents the simulation results that confirm the assertion that the mismatch between the operation of the hysteresis rods and the operation of the active control system affects the duration of damping.

CONCLUSIONS

Since CubeSat nanosatellites are usually manufactured without the radiation-resistant components, the time of their active functioning is to a great extent determined by the height of the orbit.

Nowadays the number of nanosatellites continues to grow, however they do not have any onboard passive and active devices to deorbit them. To prevent space littering and ensure the safety of the International Space Station (ISS), it is reasonable to launch such satellites into low orbits whose heights do not exceed that of the ISS.

At the same time, it is desirable to extend the time of experiments onboard nanosatellites by making their lifetime in a low orbit longer. For this purpose, we need to provide orientation of nanosatellites along the vector of the orbital motion velocity in order to reduce the ballistic coefficient.

The revealed high sensitivity of the nanosatellite motion in low orbits to the atmospheric effects, the theoretical studies of the motion nature relative to the

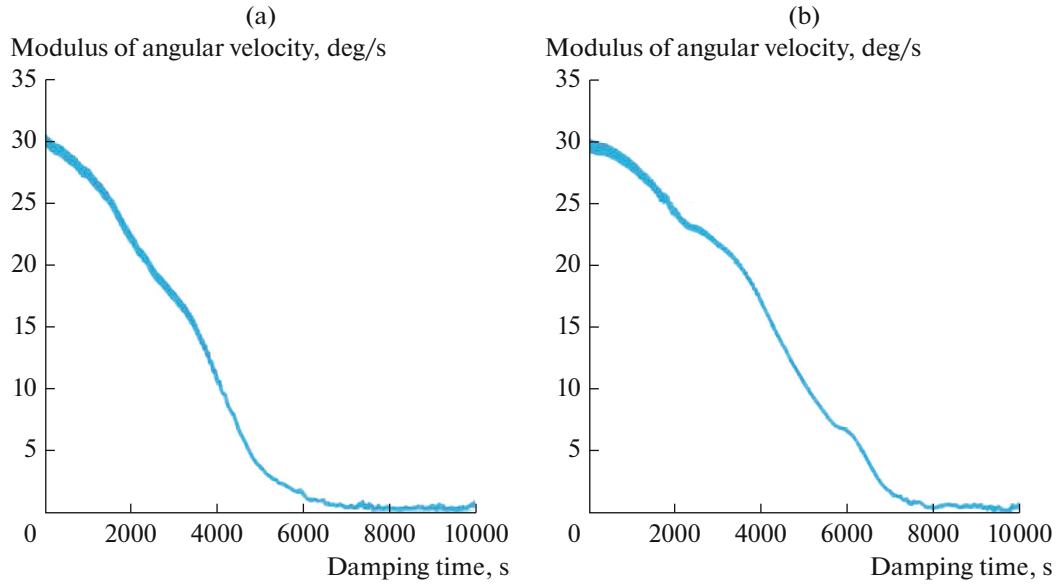

Fig. 14. Damping time of the initial angular velocity 30 deg/s for SamSat-QB50: without hysteresis rods (a) and with hysteresis rods (b).

center of mass, and the conditions for the emergence of resonant motion have made it possible to form procedures for choosing mass and inertial characteristics the use of which at the design stage ensures the technical requirements for the realization of steady motion.

The attitude stabilization system developed for aerodynamically stabilized nanosatellite SamSat-QB50 solves only the problem of dissipation of the angular momentum acquired by a nanosatellite after separation from the deployer. The cyclogram of the onboard control algorithm operation also depends on the mass and inertial characteristics of the nanosatellite; their incorrect choice can result in the failure to provide a required orientation with a required accuracy.

The emergence of resonant mode of motion almost at all heights makes it necessary to develop new methods to control the orientation in order to avoid the emergence of such motion modes.

All the features revealed in this study make it possible to take a fresh look at the nanosatellite motion dynamics and formulate new approaches to the design of the CubeSat motion and development of an integrated system of control, navigation and communication for such spacecraft.

ACKNOWLEDGMENTS

This work was supported by the Russian Science Foundation, project no. 17-79-20215.

REFERENCES

1. Kirillin, A., Belokonov, I., Timbai, I., Kramlikh, A., Melnik, M., Ustiugov, E., Egorov, A., and Shafran, S., SSAU nanosatellite project for the navigation and control technologies demonstration, *Procedia Engineering*, 2015, volume 104, pp. 97–106.
2. Shakhmatov, E., Belokonov, I., Timbai, I., Ustiugov, E., Nikitin, A., and Shafran, S., SSAU project of the nanosatellite SamSat-QB50 for monitoring the Earth's thermosphere parameters, *Procedia Engineering*, 2015, volume 104, pp. 139–146.
3. https://www.qb50.eu/.
4. Beletskii, V.V., *Dvizhenie iskusstvennogo sputnika otnositel'no tsentra mass (Motion of an Artificial Satellite Relative to the Center of Mass)*, Moscow: Nauka, 1965.
5. https://www.space-track.org
6. GOST 4401-81 *Atmosfera standartnaya. Parametry. Vvedenie* (Standard atmosphere. Parameters. Introduction) 1981-02-27. Moscow: Izvatel'stvo standartov, 1981.
7. Belokonov, I.V., Storozh, A.D., and Timbay, I.A., Modes of motion of Soyuz orbital stage after payload separation at carrying out of the short-term research experiments, *Advances in the Astronautical Sciences*, 2012, vol. 145, pp. 99–107.
8. Belokonov, I., Kramlikh, A., Timbai, I., and Lagno, O., Problems of satellite navigation and communications for nanosatellites launched as piggyback payload from the orbital stage of carrier rockets, *Proc. 21st Saint Petersburg International Conference on Integrated Navigation Systems*, 2014, pp. 407–415.
9. Belokonov, I.V., Kramlikh, A.V., and Timbai, I.A., Low-orbital transformable nanosatellite: Research of the dynamics and possibilities of navigational and communication problems solving for passive aerodynamic

stabilization, *Advances in the Astronautical Sciences*, 2015, vol. 153, pp. 383–397.

10. Yudintsev, V.V., The dynamics of the CubeSat separation from the deployer, *Polet. Obshcherossiiskii nauchno-tekhnicheskii zhurnal*, 2015, nos. 8–9, pp. 10–15.
11. Yaroshevskii, V.A., *Dvizhenie neupravlyaemogo tela v atmosphere* (Motion of an Uncontrollable Body in the Atmosphere, Moscow: Mashinostroenie, 1978.
12. Aslanov, V.S. and Boiko, V.V., Nonlinear resonant motion of an asymmetrical spacecraft in the atmosphere, *Cosmic Research*, 1985, vol. 23(3), pp. 341–347.
13. Zabolotnov, Yu.M., Lyubimov, V.V., Application of the Method Integral of Manifolds for Construction of resonant Curves for the Problem of Spacecraft Entry into the Atmosphere, 2003, *Cosmic Research*, vol. 41 (5), pp. 453–459.
14. Platus, D.H., Angle of attack convergence windward meridian rotation rate of rolling re-entry vehicles, *AIAA Journal*, vol.7, no. 12, 1969, pp. 2324–2330.
15. Aslanov, V.S., Determination of the amplitude of three-dimensional oscillations of a ballistic vehicle with a small asymmetry during atmospheric entry, 1980, *Cosmic Research*, vol. 18 (2), pp. 141–146.
16. Bogolyubov, N.N. and Mitropol'skii, Yu.A., *Asimptoticheskie metody v teorii nelineinykh kolebanii* (Asymptotic Methods in the Theory of Nonlinear Oscillations), Moscow: Nauka, 1974.
17. Rawashdeh, S.A. and Lumpp, Jr., J. E. et al., Aerodynamic stability for CubeSats at ISS orbit, *JoSS,* 2013, vol. 2, no. 1, pp. 85–104.
18. Belokonov, I. and Timbai, I., The selection of the design parameters of the aerodynamically stabilized nanosatellite of the CubeSat standard, *Procedia Engineering*, 2015, volume 104, pp. 88–96.
19. Belokonov, I., Timbai, I., and Ustyugov, E.V., Eurasian patent for invention (21) 201400132 (13) A1, Method for aerodynamic stabilization of a Cubesat and the device for its implementation, 30.07.2015.
20. Ovchinnikov, M.Yu., Pen'kov, V.I., Roldugin, D.S., and Ivanov, D.S., *Magnitnye sistemy orientatsii malykh sputnikov* (Magnetic Attitude Control Systems of Small Satellites), Moscow: IPM im. M.V. Keldysha, 2016.
21. https://gomspace.com/Shop/subsystems/solar-panels/p110-solar-panel.aspx.
22. Stickler, A.C. and Alfriend, K.T., Elementary magnetic attitude control system, *Journal of Spacecraft and Rockets*, 1976, vol. 13, no. 5, pp. 282–287.
23. Stickler, A.C., *A Magnetic Control System for Attitude Acquisition*, Ithaco, Inc., Rep. N 90345, 1972.
24. Kramlikh, A.V., Melnik, M.E., and Nikolaev, P.N., Attitude determination and stabilization algorithms of the SamSat-218D nanosatellite, *Proc. 23rd Saint Petersburg International Conference on Integrated Navigation Systems*, 2016, pp. 366–372.
25. Ovchinnikov, M.Yu., Ilyin, A.A., Kupriyanova, N.V., Pen'kov, V.I., and Selivanov A.S. Attitude dynamics of the first Russian nanosatellite TNS-0, *Acta Astronautica*, 2007, vol. 61, Is. 1–6, pp. 277–285.
26. Ovchinnikov, M. Attitude dynamics of a small-sized satellite equipped with hysteresis damper, *Advances in the Astronautical Sciences*, 2012, vol. 145, pp. 311–330.
27. Belokonov, I.V., Ivanov, D.S., Ovchinnikov, M.Yu., and Pen'kov, V.I., A system for damping the angular motion of the SamSat-QB50 nanosatellite, *Preprint of the Keldysh Institute of Applied Mathematics*, Moscow, 2015, no. 59, 28 p.